

1 **Distributive rainfall/runoff modelling to understand runoff to baseflow**
2 **proportioning and its impact on the determination of reserve requirements**
3 **of the Verlorenvlei estuarine lake, west coast, South Africa**

4

5 Andrew Watson¹, Jodie Miller¹, Manfred Fink², Sven Kralisch^{2,3}, Melanie Fleischer², and
6 Willem de Clercq³

7 *1. Department of Earth Sciences, Stellenbosch University, Private Bag X1, Matieland 7602,*
8 *South Africa*

9 *2. Department of Geoinformatics, Friedrich-Schiller-University Jena, Loebdergraben 32,*
10 *07743 Jena, Germany*

11 *3. German Aerospace Center (DLR), Institute of Data Science, Maelzerstraße 3, 07745 Jena,*
12 *Germany*

13 *4. Stellenbosch Water Institute, Stellenbosch University, Private Bag X1, Matieland, 7602,*
14 *South Africa*

15

16 **Keywords:** rainfall/runoff modelling, Verlorenvlei reserve, J2000

17 **Abstract**

18 River systems that support high biodiversity profiles are conservation priorities world-wide.
19 Understanding river eco-system thresholds to low flow conditions is important for the
20 conservation of these systems. While climatic variations are likely to impact the streamflow
21 variability of many river courses into the future, understanding specific river flow dynamics
22 with regard to streamflow variability and aquifer baseflow contributions are central to the
23 implementation of protection strategies. While streamflow is a measurable quantity, baseflow
24 has to be estimated or calculated through the incorporation of hydrogeological variables. In

25 this study, the groundwater components within the J2000 rainfall/runoff model were distributed
26 to provide daily baseflow and streamflow estimates needed for reserve determination. The
27 modelling approach was applied to the RAMSAR-listed Verlorenvlei estuarine lake system on
28 the west coast of South Africa which is under threat due to agricultural expansion and climatic
29 fluctuations. The sub-catchment consists of four main tributaries, the Krom Antonies, Hol,
30 Bergvallei and Kruismans. Of these, the Krom Antonies was initially presumed the largest
31 baseflow contributor, but was shown to have significant streamflow variability, attributed to
32 the highly conductive nature of the Table Mountain Group sandstones and quaternary
33 sediments. Instead, the Bergvallei was identified as the major contributor of baseflow. The Hol
34 was the least susceptible to streamflow fluctuations due to the higher baseflow proportion
35 (56%), as well as the dominance of less conductive Malmesbury shales that underlie it. The
36 estimated flow exceedance probabilities indicated that during the 2008-2017 wet cycle average
37 lake inflows exceeded the average evaporation demand. During the 1997-2007 dry cycle,
38 average lake inflows are exceeded 85 % of the time by the evaporation demand. The
39 exceedance probabilities estimated here suggest that inflows from the four main tributaries are
40 not enough to support Verlorenvlei, with the evaporation demand of the entire lake being met
41 only 35 % of the time. This highlights the importance of low occurrence events for filling up
42 Verlorenvlei, allowing for regeneration of lake-supported ecosystems. As climate change
43 drives increased temperatures and rainfall variability, the length of dry cycles are likely to
44 increase into the future and result in the lake drying up more frequently. For this reason, it is
45 important to ensure that water resources are not overallocated during wet cycles, hindering
46 ecosystem regeneration and prolonging the length of these dry cycle conditions.

47 **1. Introduction**

48 Functioning river systems offer numerous economic and social benefits to society including
49 water supply, nutrient cycling and disturbance regulation amongst others (Nelson et al., 2009;
50 Postel and Carpenter, 1997). As a result, many countries worldwide have endeavoured to
51 protect river ecosystems, although only after provision has been made for basic human needs
52 (Gleick, 2003; Ridoutt and Pfister, 2010). However, the implementation of river protection has
53 been problematic, because many river courses and flow regimes have been severely altered due
54 to socio-economic development (O'Keeffe, 2009; Richter, 2010). River health problems
55 thought to only result from low-flow conditions and if minimum flows were kept above a
56 critical level, the river's ecosystem would be protected (Poff et al., 1997). It is now recognised
57 that a more natural flow regime, which includes floods as well as low and medium flow
58 conditions, is required for sufficient ecosystem functioning (Bunn and Arthington, 2002; Olden
59 and Naiman, 2010; Postel and Richter, 2012). For these reasons, before protection strategies
60 can be developed or implemented for a river system, a comprehensive understanding of the
61 river flow regime dynamics is necessary.

62 River flow regime dynamics include consideration of not just the surface water in the river but
63 also other water contributions including runoff, interflow and baseflow which are all essential
64 for the maintenance of the discharge requirements. Taken together these factors all contribute
65 to the determination of what is called the ecological reserve, the minimum environmental
66 conditions needed to maintain the ecological health of a river system (Acreman and Dunbar,
67 2004; Hughes, 2001). A variety of different methods have been developed to incorporate
68 various river health factors into ecological reserve determination (Bragg et al., 2005). One of
69 the simplest and most widely applied, is where compensation flows are set below reservoirs
70 and weirs, using flow duration curves to derive mean flow or flow exceedance probabilities

71 (e.g. Harman and Stewardson, 2005). This approach focusses purely on hydrological indices,
72 which are rarely ecologically valid(e.g. Barker and Kirmond, 1998).

73 More comprehensive ecological reserve estimates such as functional analysis are focused on
74 the whole ecosystem, including both hydraulic and ecological data (e.g. ELOHA: Poff et al.,
75 2010; Building Block Methodology: King and Louw, 1998). While these methods consider that
76 a variety of low, medium and high flow events are important for maintaining ecosystem
77 diversity, they require specific data regarding the hydrology and ecology of a river system,
78 which in many cases does not exist, has not been recorded continuously or for sufficient
79 duration (Acreman and Dunbar, 2004). To speed up ecological reserve determination, river
80 flow records have been used to analyse natural seasonality and variability of flows (e.g. Hughes
81 and Hannart, 2003). However, this approach requires long-term streamflow and baseflow
82 timeseries. Whilst streamflow is a measurable quantity subject to a gauging station being in
83 place, baseflow has to be modelled based on hydrological and hydrogeological variables.

84 Rainfall/runoff models can be used to calculate hydrological variables using distributive
85 surface water components (e.g. J2000: Krause, 2001) but the groundwater components are
86 generally lumped within conventional modelling frameworks. In contrast, groundwater
87 models, which distribute groundwater variables (e.g. MODFLOW: Harbaugh, Arlen, 2005),
88 are frequently setup to lump climate components. In order to accurately model daily baseflow,
89 which is needed for reserve determination, modelling systems need to be setup such that both
90 groundwater and climate variables are treated in a distributive manner (e.g Bauer et al., 2006;
91 Kim et al., 2008). Rainfall/runoff models, which use Hydrological Response Units (HRUs) as
92 an entity of homogenous climate, rainfall, soil and landuse properties (Flügel, 1995), are able
93 to reproduce hydrographs through model calibration (Wagener and Wheater, 2006). However,
94 they are rarely able to correctly proportion runoff and baseflow components (e.g. Willems,
95 2009). To correctly determine groundwater baseflow using rainfall/runoff models such as the

96 J2000, aquifer components need to be distributed. This can be achieved using net recharge and
97 hydraulic conductivity collected through aquifer testing or groundwater modelling.

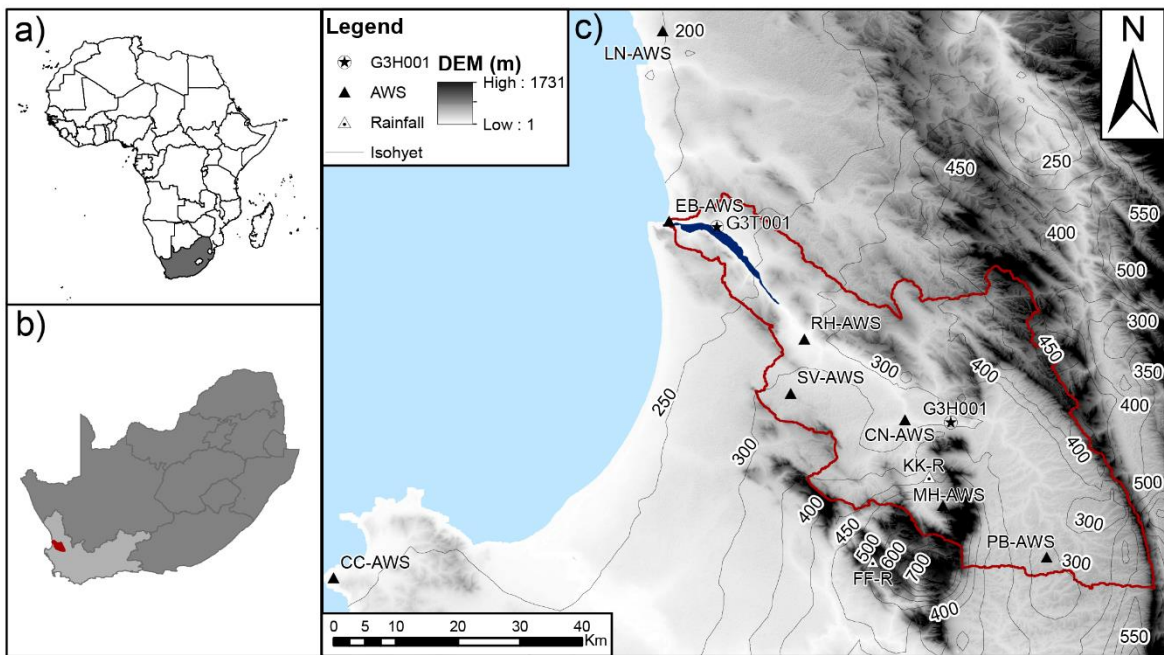
98 To better understand river flow variability, a rainfall/runoff model was distributed to
99 incorporate aquifer hydraulic conductivity within model HRUs using calibrated values from a
100 MODFLOW groundwater model (Watson, 2018). The rainfall/runoff model used was J2000
101 as this model had previously been set up in the region and model variables were well
102 established (e.g Bugan, 2014; Schulz et al., 2013). The model was setup for the RAMSAR
103 listed Verlorenvlei estuarine lake on the west coast of South Africa, which is under threat from
104 climate change, agricultural expansion and mining exploration. While the estuarine lake's
105 importance is well documented (Martens et al., 1996; Wishart, 2000), the lake's reserve is not
106 well understood, due to the lack of streamflow and baseflow estimates for the main feeding
107 tributaries of the system. The modelling framework developed in this study aimed to
108 understand the flow variability of the lake's feeding tributaries, to provide the hydrological
109 components (baseflow and runoff proportioning) of the tributaries needed to understand the
110 lake reserve. The surface water and groundwater components of the model were calibrated for
111 two different tributaries which were believed to be the main source of runoff and baseflow for
112 the sub-catchment. The baseflow and runoff rates calculated from the model indicate not only
113 that the lake system cannot be sustained by baseflow during low flow periods but also that the
114 initial understanding of which tributaries are key to the sustainability of the lake system was
115 not correct. The results have important implications for how we understand water dynamics in
116 water stressed catchments and the sustainability of ecological systems in these environments.

117 **2. Study site**

118 Verlorenvlei is an estuarine lake situated on the west coast of South Africa, approximately 150
119 km north of the metropolitan city of Cape Town (Fig. 1). The west coast, which is situated in

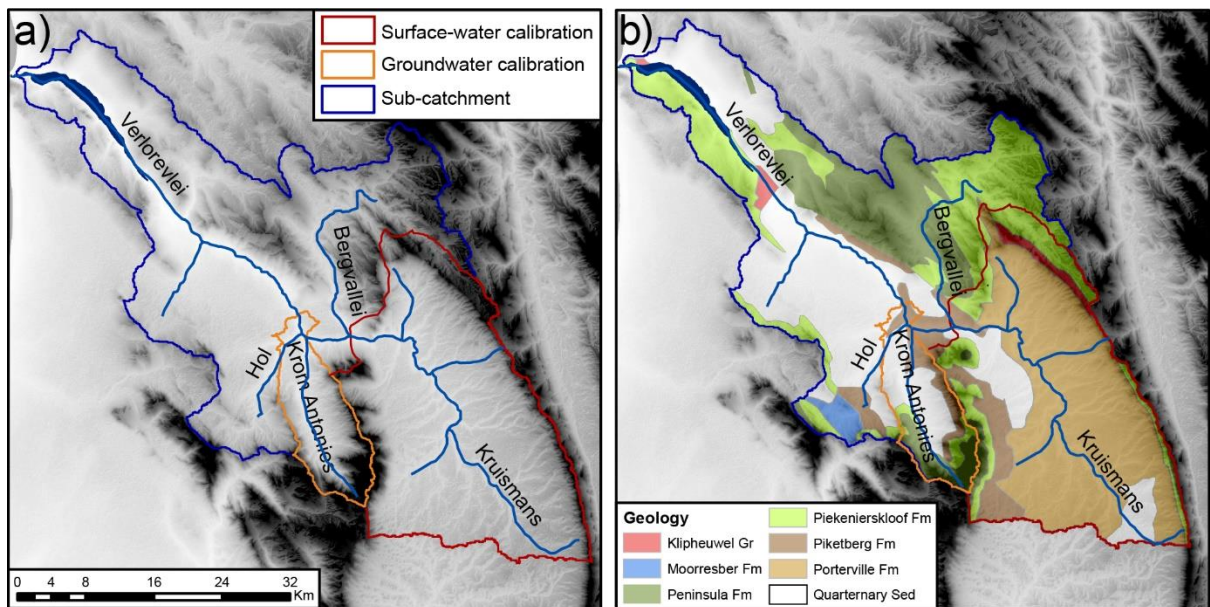
120 the Western Cape Province of South Africa, is subject to a Mediterranean climate where the
121 majority of rainfall is received between May to September. The Verlorenvlei lake, which is
122 approximately 15 km² in size draining a watershed of 1832 km², forms the southern sub-
123 catchment of the Olifants/Doorn water management area (WMA). The lake hosts both Karroid
124 and Fynbos biomes, with a variety of vegetation types (e.g Arid Estuarine Saltmarsh, Cape
125 Inland Salt pans) sensitive to reduced inflows of freshwater (Helme, 2007). A sandbar created
126 around a sandstone outcrop (Table Mountain Group) allows for an intermittent connection
127 between salt and fresh water. During storms or extremely high tides, water scours the sand bar
128 allowing for a tidal exchange, with a constant inflow of salt water continuing until the inflow
129 velocity decreases enough for a new sand bar to form (Sinclair et al., 1986).

130 The lake is supplied by four main tributaries which are the Krom Antonies, Bergvallei, Hol and
131 Kruismans (Fig. 2). The main freshwater sources are presumed to be the Krom Antonies and
132 the Bergvallei, which drain the mountainous regions to the south (Piketberg) and north of the
133 sub-catchment respectfully (Sigidi, 2018). The Hol and Kruismans tributaries are variably
134 saline (Sigidi, 2018), due to high evaporation rates in the valley. Average daily temperatures
135 during summer within the sub-catchment are between 20-30 °C, with estimated potential
136 evaporation rates of 4 to 6 mm.d⁻¹ (Muche et al., 2018). In comparison, winter daily average
137 temperatures are between 12-20 °C, with estimated potential evaporation rates of 1 to 3 mm.d⁻¹
138 ¹ (Muche et al., 2018).



139

140 Figure 1: a) Location of South Africa, b) the location of the study catchment within the Western
 141 Cape and c) the extend of the Verlorenvlei sub-catchment with the climate stations, gauging
 142 station (G3H001), measured lake water level (G3T001) and rainfall isohets

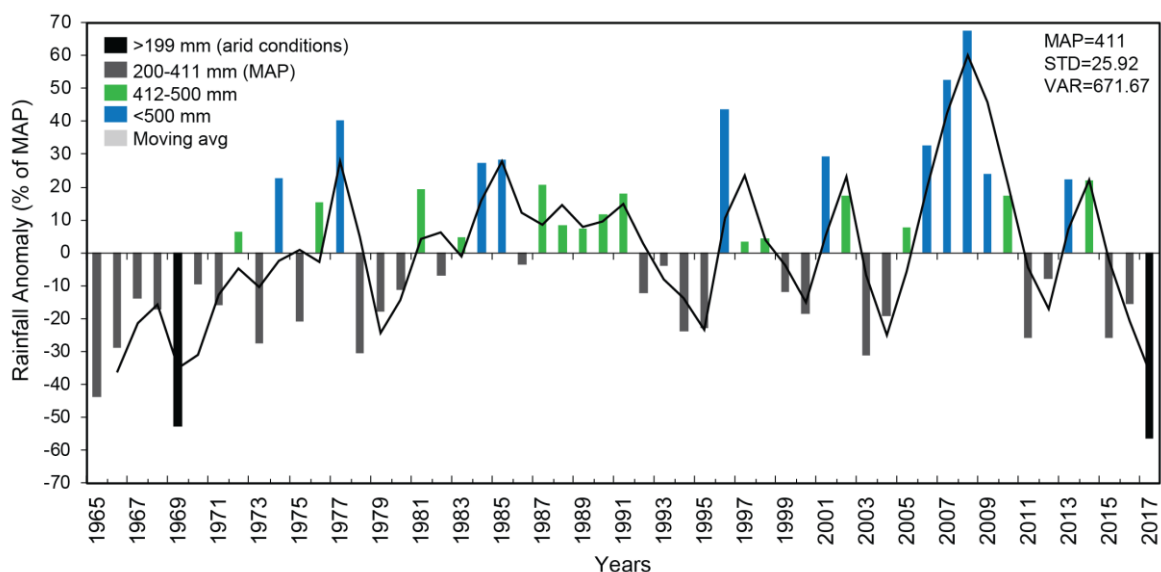


143

144 Figure 2: a) The Verlorenvlei sub-catchment with the surface water calibration tributary
 145 (Kruismans) and groundwater calibration tributary (Krom Antonies) and b) the hydrogeology
 146 of the sub-catchment with Malmesbury shale formations (Klipheuwel, Mooresberg, Porterville,

147 Piketberg), Table Mountain Group formations (Peninsula, Piekenierskloof) and quaternary
148 sediments

149 Rainfall for the sub-catchment, recorded over the past 52 years by local farmers at KK-R (Fig.
150 1) shows large yearly variability (26%) between the Mean Annual Precipitation (MAP)(411
151 and measured rainfall (Fig. 3). Where rainfall was greater than 500 mm.yr^{-1} (2006-2010), it is
152 presumed that the lake is supported by a constant influx of streamflow from the feeding
153 tributaries. Where rainfall was less than 50 % of the MAP (1965-1969 and 2015-2017),
154 concerns over the amount of streamflow required to support the lake have been raised.



155
156 Figure 3: The difference between MAP and measured rainfall (plotted as rainfall anomaly) for
157 52 years (1965-2017) at location KK-R in the valley of the Krom Antonies (after Watson *et*
158 *al.*, 2018).

159 While rainfall varies greatly between years in the sub-catchment, it is also spatially impacted
160 by elevational differences. The catchment valley which receives the least MAP $100-350 \text{ mm.yr}^{-1}$
161 ¹ (Lynch, 2004), is between 0-350 masl and is comprised of quaternary sediments that vary in
162 texture, although the majority of the sediments in the sub-catchment are sandy in nature. The

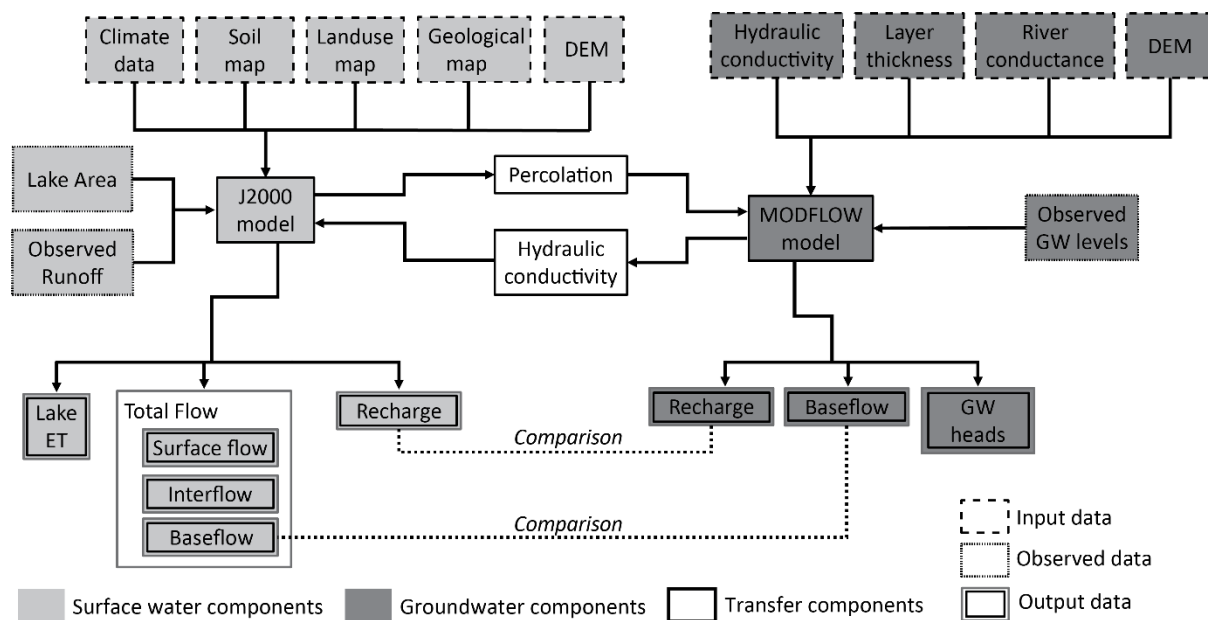
163 higher relief mountainous regions of the sub-catchment between 400-1300 masl receive the
164 highest MAP 400-800 mm.yr⁻¹ (Lynch, 2004), are mainly comprised of fractured TMG
165 sandstones, (youngest to oldest): Peninsula, Graafwater (not shown), and Piekernerskloof
166 formations (Fig. 2) (Johnson et al., 2006). Underlying the sandstones and quaternary sediments
167 are the MG shales, which are comprised of the Mooresberg, Piketberg and Klipheuwel
168 formations (Fig. 2) (Rozendaal and Gresse, 1994). Agriculture is the dominant water user in
169 the sub-catchment with an estimated usage of 20 % of the total recharge (DWAF, 2003;
170 Watson, 2018), with the main food crop being potatoes. The MG shales and quaternary
171 sediments, which host the secondary and primary aquifer respectfully, are frequently used to
172 supplement irrigation during the summer months of the year. During winter, the majority of
173 the irrigation water needed for crop growth is supplied by the sub-catchment tributaries or the
174 lake itself. The impact of irrigation on the lake is still regarded as minimal (Meinhardt et al.,
175 2018) but requires future investigation. For additional information regarding the study site refer
176 to Watson *et al.*, (2018).

177 **3. Methodology**

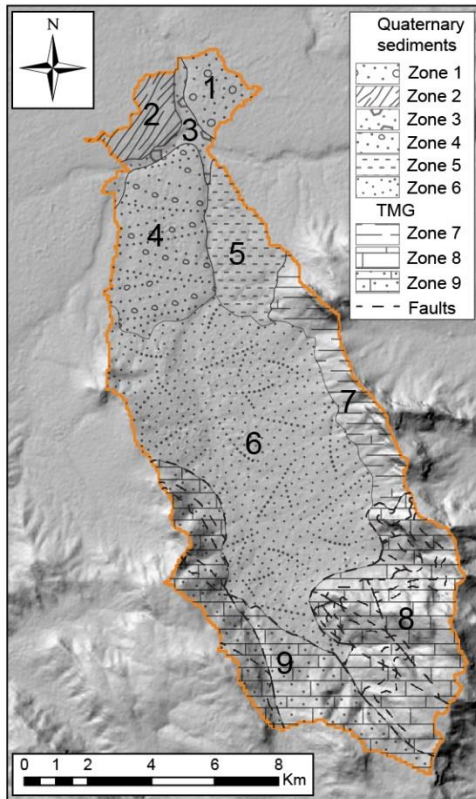
178 In this study, the J2000 coding was adapted to incorporate distributive groundwater
179 components for the model HRU's (Fig. 4). This was done by aligning the MODFLOW recharge
180 estimates with those of the J2000, through adjustment of aquifer hydraulic conductivity from
181 the MODFLOW groundwater model of the Krom Antonies (Watson, 2018) (Fig. 5). The
182 assigned hydraulic conductivity for each geological formation was thereafter transferred across
183 the entire J2000 model of the sub-catchment. The adaption applied to the groundwater
184 components influenced the proportioning of water routed to runoff and baseflow within the
185 J2000 model. To validate the outputs of the model, an empirical mode decomposition (EMD)
186 (Huang et al., 1998) was applied to compute the proportion of variation in discharge timeseries

187 that attributed to a high and low water level change at the sub-catchment outlet. The streamflow
 188 estimates were thereafter compared with the lake evaporation demand, to understand the sub-
 189 catchment water balance.

190 The J2000 model incorporated distributive climate, soil, landuse and hydrogeological
 191 information, with aquifer hydraulic conductivity transferred from MODFLOW as described
 192 above (Fig. 4). The measured streamflow was used to both calibrate and validate the model,
 193 with the landuse dataset being selected according to the period of measured streamflow.
 194 Changes in the recorded lake level were used alongside remote sensing to estimate the lake
 195 evaporation rate. The impact of irrigation was not included in the model, as there is not enough
 196 information available regarding agricultural water use. This is currently one of the major
 197 limitations with the study approach presented here and will be the focus of future work. The
 198 HRU delineation, model regionalisation, water balance calculations, lateral and reach routing
 199 as well as the lake evaporation procedure are presented. Thereafter the input data for the model,
 200 the calibration and validation procedures as well as the EMD protocol used, is described.



201 Figure 4: Schematic of the model structure, showing the processors simulated by the J2000 and
 202 MODFLOW and the components that were transferred from the MODFLOW model



204

205 Figure 5: The aquifer hydraulic zones used for the groundwater calibration of the J2000 (after
 206 Watson, 2018)

207 **3.1 Hydrological Response Unit Delineation**

208 HRUs and stream segments (reaches) are used within the J2000 model for distributive
 209 topographic and physiological modelling. In this study, the HRU delineation made use of a
 210 digital elevation model, with slope, aspect, solar radiation index, mass balance index and
 211 topographic wetness being derived. Before the delineation process, gaps within the digital
 212 elevation model were filled using a standard fill algorithm from ArcInfo (Jenson and
 213 Domingue, 1988). The AML (ArcMarkupLanguage) automated tool (Pfennig et al., 2009) was
 214 used for the HRU delineation, with between 13 and 14 HRUs/km² being defined
 215 (Pfannschmidt, 2008). After the delineation of HRUs, dominant soil, land use and geology
 216 properties were assigned to each. The hydrological topology was defined for each HRU by
 217 identifying the adjacent HRUs or stream segments that received water fluxes.

218 **3.2 Model regionalisation**

219 Rainfall and relative humidity are the two main parameters that are regionalised within the
220 J2000 model. While a direct regionalisation using an inverse-distance method (IDW) and the
221 elevation of each HRU can be applied to rainfall data, the regionalisation of relative humidity
222 requires the calculation of absolute humidity. The regionalisation of rainfall records was
223 applied by defining the number of weather station records available and estimating the
224 influence on the rainfall amount for each HRU. A weighting for each station using the distance
225 of each station to the area of interest was applied to each rainfall record, using an elevation
226 correction factor (Watson et al., 2018). The relative humidity and air temperature measured at
227 set weather stations were used to calculate the absolute humidity. Absolute humidity was
228 thereafter regionalised using the IDW method, station and HRU elevation. After the
229 regionalisation had been applied, the absolute humidity was converted back to relative
230 humidity through calculation of saturated vapor pressure and the maximum humidity.

231 **3.3 Water balance calculations**

232 The J2000 model is divided into calculations that impact surface water and groundwater
233 processors. The J2000 model distributes the regionalised precipitation (P) calculated for each
234 HRU using a water balance defined as:

$$P = R + Int_{max} + ETR + \Delta Soil_{sat} \quad (1)$$

235 where R is runoff (mm) (RD1 - surface runoff; RD2 - interflow), Int_{max} is vegetation canopy
236 interception (mm), ETR is 'real' evapotranspiration and $\Delta Soil_{sat}$ is change in soil saturation.
237 The surface water processes have an impact on the amount of modelled runoff and interflow,
238 while the groundwater processors influence the upper and lower groundwater flow
239 components.

240 **3.3.1 Surface water components**

241 Potential evaporation (ETP) within the J2000 model is calculated using the Penman Monteith
242 equation. Before evaporation was calculated for each HRU, interception was subtracted from
243 precipitation using the leaf area index and leaf storage capacity for vegetation (a_rain)
244 (Supplementary: Table 1). Evaporation within the model considers several variables that
245 influence the overall modelled evaporation. Firstly, evaporation is influenced by a slope factor,
246 which was used to reduce ETP based on a linear function. Secondly, the model assumed that
247 vegetation transpires until a particular soil moisture content where ETP is reached, after which
248 modelled evaporation was reduced proportionally to the ETP, until it became zero at the
249 permanent wilting point.

250 The soil module in the J2000 model is divided up into processing and storage units. Processing
251 units in the soil module include soil-water infiltration and evapotranspiration, while storage
252 units include middle pore storage (MPS), large pore storage (LPS) and depression storage. The
253 infiltrated precipitation was calculated using the relative saturation of the soil, and its maximum
254 infiltration rate (SoilMaxInfSummer and SoilMaxInfWinter) (Supplementary: Table 1).
255 Surface runoff was generated when the maximum infiltration threshold was exceeded. The
256 amount of water leaving LPS, which can contribute to recharge, was dependant on soil
257 saturation and the filling of LPS via infiltrated precipitation. Net recharge (R_{net}) was estimated
258 using the hydraulic conductivity ($SoilMaxPerc$), the outflow from LPS (LPS_{out}) and the slope
259 ($slope$) of the HRU according to:

$$R_{net} = LPS_{out} \times (1 - \tan(slope) \cdot SoilMaxPerc) \quad (2)$$

260 The hydraulic conductivity, $SoilMaxPerc$ and the adjusted LPS_{out} were thereafter used to
261 calculate interflow (IT_f) according to:

$$IT_f = LPS_{out} \times (\tan(slope) \cdot SoilMaxPerc) \quad (3)$$

262 with the interflow calculated representing the sub-surface runoff component RD2 and is routed
 263 as runoff within the model.

264 **3.3.2 Groundwater components**

265 The J2000 model for the Verlorenvlei sub-catchment was set up with two different geological
 266 reservoirs: (1) the primary aquifer (upper groundwater reservoir - RG1), which consists of
 267 quaternary sediments with a high permeability; and (2) the secondary aquifer (lower
 268 groundwater reservoir- RG2), made up of MG shales and TMG sandstones (Table 1).

Aquifer	Formation	Type	RG1_max (mm)	RG2_max (mm)	RG1_k (d)	RG2_k (d)	RG1_active (n/a)	Kf_geo (mm/d)	depthRG1 (cm)
Primary	Quaternary Sediments	Sediments	50	700	100	431	1	500	1750
Secondary/MG	Moorresberg Formation	Shale Greywacke	0	580	0	350	0	950	1750
Secondary/MG	Porterville Formation	Shale Greywacke	0	560	0	335	0	2	1750
Secondary/MG	Piketberg Formation	Shale Greywacke	0	1000	0	600	0	950	1750
Secondary/MG	Klipheuwel Group	Shale Greywacke	0	500	0	300	0	950	1750
Secondary/TMG	Peninsula Formation	Sandstone	0	1000	0	600	0	950	1750
Secondary/TMG	Piekenierskloof Formation	Sandstone	0	600	0	400	0	1	1750

269
 270 Table 1: The J2000 hydrogeological parameters RG1_max, RG2_max, RG1_k, RG2_Kf_geo
 271 and depthRG1 assigned to the primary and secondary aquifer formations for the Verlorenvlei
 272 sub-catchment

273 The model therefore considered two baseflow components, a fast one from the RG1 and a
 274 slower one from RG2. The filling of the groundwater reservoirs was done by net recharge, with
 275 emptying of the reservoirs possible by lateral subterranean runoff as well as capillary action in
 276 the unsaturated zone. Each groundwater reservoir was parameterised separately using the
 277 maximum storage capacity (maxRG1 and maxRG2) and the retention coefficients for each
 278 reservoir (*recRG1* and *recRG2*). The outflow from the reservoirs was determined as a function
 279 of the actual filling (*actRG1* and *actRG2*) of the reservoirs and a linear drain function.
 280 Calibration parameters *recRG1* and *recRG2* are storage residence time parameters. The
 281 outflow from each reservoir was defined as:

$$OutRG1 = \frac{1}{gwRG1Fact \times recRG1} \times actRG1 \quad (4)$$

$$OutRG2 = \frac{1}{gwRG2Fact \times recRG2} \times actRG2 \quad (5)$$

282 where $OutRG1$ is the outflow from the upper reservoir, $OutRG2$ is the outflow from the lower
 283 reservoir and $gwRG1Fact/ gwRG2Fact$ are calibration parameters for the upper and lower
 284 reservoir used to determine the outflow from each reservoir. To allocate the quantity of net
 285 recharge between the upper (RG1) and lower (RG2) groundwater reservoirs, a calibration
 286 coefficient $gwRG1RG2sdist$ was used to distribute the net recharge for each HRU using the
 287 HRU slope. The influx of groundwater into the shallow reservoir ($inRG1$) was defined as:

$$inRG1 = R_{net} \times (1 - (1 - \tan(slope))) \times gwRG1RG2sdist \quad (6)$$

288 The influx of net recharge into the lower groundwater reservoir ($inRG2$) was defined as:

$$inRG2 = R_{net} \times (1 - \tan(slope)) \times gwRG1RG2sdist \quad (7)$$

289 with the combination of $OutRG1$ and $OutRG2$ representing the baseflow component that is
 290 routed as an outflow from the model.

291 **3.4 Lateral and reach routing**

292 Lateral routing was responsible for water transfer within the model and included HRU influxes
 293 and discharge through routing of cascading HRUs from the upper catchment to the exit stream.
 294 HRUs were either able to drain into multiple receiving HRUs or into reach segments, where
 295 the topographic ID within the HRU dataset determined the drain order. The reach routing
 296 module was used to determine the flow within the channels of the river using the kinematic
 297 wave equation and calculations of flow according to Manning and Strickler. The river
 298 discharge was determined using the roughness coefficient of the stream (Manning roughness),
 299 the slope and width of the river channel and calculations of flow velocity and hydraulic radius
 300 calculated during model simulations.

301 **3.5 Calculations of lake evaporation rate**

302 The lake evaporation rate was based on the ETP calculated by the J2000 and an estimated lake
303 surface area. The lake was modelled as a unique HRU (water as the land-cover type), with a
304 variable area which was estimated using remote sensing data from Landsat 8 and Sentinel-2
305 and the measured lake water level at G3T001 (Fig. 1). To infill lake surface area when remote
306 sensing data was not available, a relationship was created between the estimated lake's surface
307 area and the measured water level between 2015-2017. Where lake water level data was not
308 available (before 1999), an average long-term monthly value was used for the lake evaporation
309 calculations.

310 **3.6 J2000 Input data**

311 ***3.6.1 Surface water parameters***

312 Climate and rainfall: Rainfall, windspeed, relative humidity, solar radiation and air temperature
313 were monitored by Automated Weather Stations (AWS) within and outside of the study
314 catchment (Fig. 1). Of the climate and rainfall data used during the surface water modelling
315 (Watson et al., 2018), data was sourced from seven AWS's of which four stations were owned
316 by the South African Weather Service (SAWS) and three by the Agricultural Research Council
317 (ARC). Two stations that were installed for the surface water modelling, namely Moutonshoek
318 (M-AWS) and Confluence (CN-AWS) were used for climate and rainfall validation due to their
319 short record length. Additional rainfall data collected by farmers at high elevation at location
320 FF-R and within the middle of the catchment at KK-R were used to improve the climate and
321 rainfall network density.

322 Landuse classification: The vegetation and landuse dataset that was used for the sub-catchment
323 (CSIR, 2009) included five different landuse classes: 1) wetlands and waterbodies, 2)
324 cultivated (temporary, commercial, dryland), 3) shrubland and low fynbos, 4) thicket,

325 bushveld, bush clumps and high fynbos and 5) cultivated (permanent, commercial, irrigated).
326 Each different landuse class was assigned an albedo, root depth and seal grade value based on
327 previous studies (Steudel et al., 2015)(Supplementary: Table 2). The Leaf Area Index (LAI)
328 and vegetation height varies by growing season with different values of each for the particular
329 growing season. While surface resistance of the landuse varied monthly within the model, the
330 values only vary significantly between growing seasons.

331 Soil dataset: The Harmonized World Soil Database (HWSD) v1.2 (Batjes et al., 2012) was the
332 input soil dataset, with nine different soil forms within the sub-catchment (Supplementary:
333 Table 3). Within the HWSD, soil depth, soil texture and granulometry were used to calculate
334 and assign soil parameters within the J2000 model. MPS and LPS which differ in terms of the
335 soil structure and pore size were determined in Watson et al. (2018), using pedotransfer
336 functions within the HYDRUS model (Supplementary: Table 3).

337 Streamflow and water levels: Streamflow, measured at the Department of Water Affairs
338 (DWA) gauging station G3H001 between 1970-2009, at the outlet of the Kruismans tributary
339 (Het Kruis) (Fig 1 and 3), was used for surface water calibration. The G3H001 two-stage weir
340 could record a maximum flow rate of $3.68 \text{ m}^2 \cdot \text{s}^{-1}$ due to the capacity limitations of the structure.
341 After 2009, the G3H001 structure was decommissioned due to structural damage, although
342 repairs are expected in the near future due to increasing concerns regarding the influx of
343 freshwater into the lake. Water levels measured at the sub-catchment outlet at DWA station
344 G3T001 (Fig 1) between 1994 to 2018 were used for EMD filtering.

345 **3.6.2 Groundwater parameters**

346 Net recharge and hydraulic conductivity: The hydraulic conductivity values used for the
347 groundwater component adaptation were collected from detailed MODFLOW modelling of the
348 Krom Antonies tributary (Fig. 5) (Watson, 2018). The net recharge and aquifer hydraulic

349 conductivity for the Krom Antonies tributary, was estimated through PEST autocalibration
350 using hydraulic conductivities from previous studies (SRK, 2009; UMVOTO-SRK, 2000) and
351 potential recharge estimates (Watson et al., 2018).

352 Hydrogeology: Within the hydrogeological dataset, parameters assigned include maximum
353 storage capacity (RG1 and RG2), storage coefficients (RG1 and RG2), the minimum
354 permeability/maximum percolation (Kf_geo of RG1 and RG2) and depth of the upper
355 groundwater reservoir (depthRG1). The maximum storage capacity was determined using an
356 average thickness of each aquifer and the total number of voids and cavities, where the primary
357 aquifer thickness was assumed to be between 15-20 m (Conrad et al., 2004), and the secondary
358 aquifer between 80-200 m (SRK, 2009). The maximum percolation of the different geological
359 formations was assigned hydraulic conductivities using the groundwater model for the Krom
360 Antonies sub-catchment (Watson, 2018). The J2000 geological formations were assigned
361 conductivities to modify the maximum percolation value to ensure internal consistency with
362 recharge values calculated using MODFLOW (Table 1).

363 **3.7 J2000 model calibration**

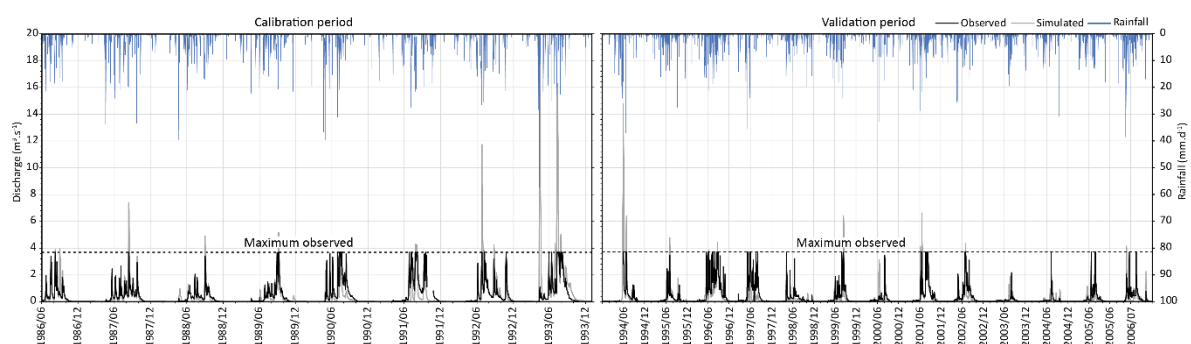
364 ***3.7.1 Model sensitivity***

365 The J2000 sensitivity analysis for Verlorenvlei sub-catchment was presented in Watson *et al.*,
366 (2018) and therefore only a short summary is presented here. In this study, parameters that
367 were used to control the ratio of interflow to percolation were adjusted, which in the J2000
368 model include a slope (SoilLatVertDist) and max percolation value. The sensitivity analysis
369 conducted by Watson *et al.*, (2018) showed that for high flow conditions (E2) (Nash-Sutcliffe
370 efficiency in its standard squared), model outputs are most sensitive to the slope factor, while
371 for low flow conditions (E1) (modified Nash-Sutcliffe efficiency in a linear form) the model
372 outputs were most sensitive to the maximum infiltration rate of the soil (ie. the parameter

373 maxInfiltrationWet) (Supplementary: Figure 1). The max percolation was moderately sensitive
374 during wet and dry conditions, and together with the slope factor, controlled the interflow to
375 percolation portioning that was calibrated in this study.

376 **3.7.2 Surface water calibration**

377 The surface water parameters of the model were calibrated for the Kruismans tributary (688
378 km²) (Fig. 3) using the gauging data from G3H001 (Fig. 6 and Table 1). The streamflow data
379 used for the calibration was between 1986-1993, with model validation between 1994 to 2007
380 (Fig. 6). This specific calibration period was selected due to the wide range of different runoff
381 conditions experienced at the station, with both low and high flow events being recorded. For
382 the calibration, the modelled discharge was manipulated in the same fashion, with a DT limit
383 (discharge table) of 3.68 m³/s, so that the tributary streamflow behaved as measured discharge.



384
385 Figure 6: The surface water calibration (1986-1993) and validation (1994-2006) of the J2000
386 model using gauging data from the G3H001

387 An automated model calibration was performed using the “Nondominating Sorting Genetic
388 Algorithm II” (NSGA-II) multi-objective optimisation method (Deb et al., 2002) with 1023
389 model runs being performed. Narrow ranges of calibration parameters (FC_Adaptation,
390 AC_Adaptation, soilMAXDPS, gwRG1Fact and gwRG2Fact) were chosen to (1) ensure that
391 the modelled recharge from J2000 was within an order of magnitude of recharge from the
392 MODFLOW model; (2) to achieve a representative sub-catchment hydrograph. As objective

393 functions, the E2, E1 and the average bias in % (Pbias) were utilized for the calibration (Krause
394 et al., 2005) (Table 2). The choice of the optimized parameter set was made to ensure that E2
395 was better than 0.57 (best value was 0.57) and the Pbias better than 5% (Table 1). From the
396 automated calibration, 308 parameter sets were determined with the best E1 being chosen to
397 ensure that the model is representative of low flow conditions (Table 1).

398 **3.7.3 Model validation**

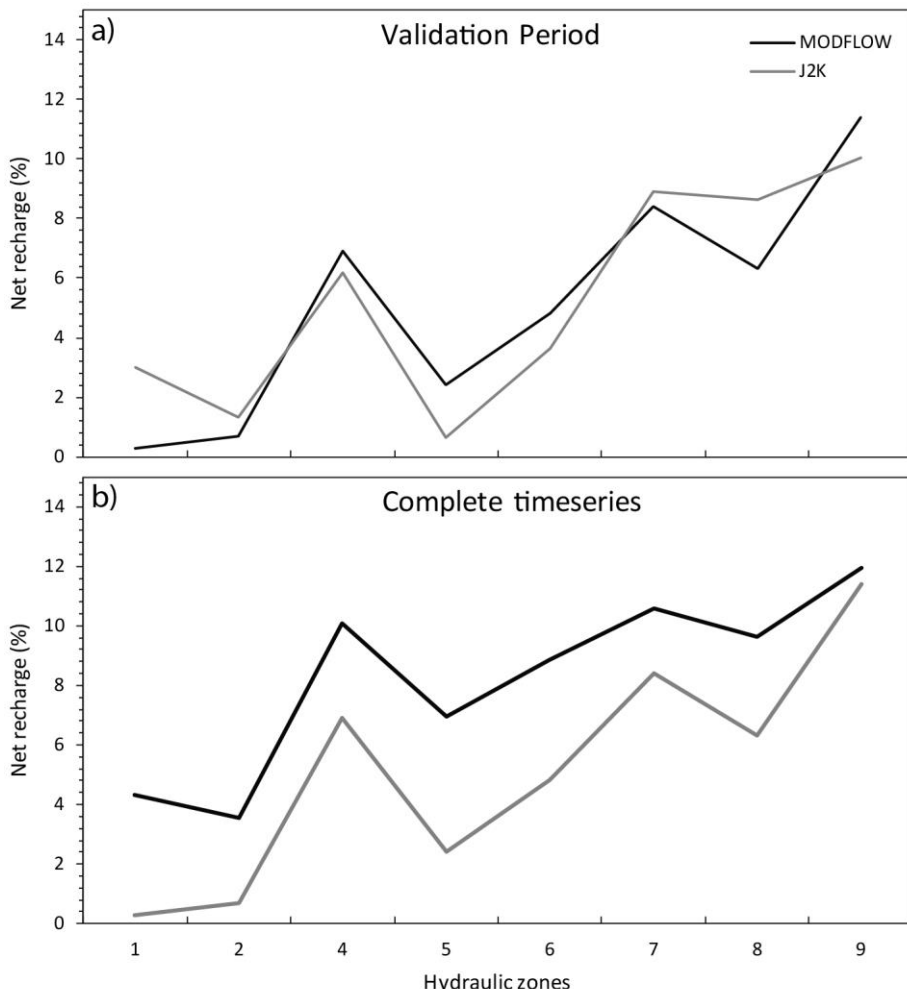
399 Observed vs modelled streamflow: For the surface water model validation, the streamflow
400 records between 1994-2007 were used, where absolute values (E1) and squared differences
401 (E2) of the Nash Sutcliffe efficiency were reported. The Pbias was also used as an objective
402 function to report the model performance by comparison between measured and modelled
403 streamflow (Table 2). Although gauging station limitations resulted in good objective functions
404 from the model, the performance of objective functions E1, E2, Pbias reduced between the
405 validation and calibration period (Table 2). During the calibration period there was a good fit
406 between modelled and measured streamflow (Pbias=-1.82), with a significant difference
407 between modelled and measured streamflow during the validation period (Pbias=-19.2). The
408 calibration was performed over a wet cycle (1986-1997), which resulted in a more common
409 occurrence of streamflow events that exceeded $3.68 \text{ m}^3 \cdot \text{s}^{-1}$, thereby reducing the number of
410 calibration points. In contrast the validation was performed over a dry cycle (1997-2007),
411 which resulted in more data points as few streamflow events exceeded $3.68 \text{ m}^3 \cdot \text{s}^{-1}$.

	Calibration 1987-1993	Validation 1994-2007
E1	0.55	0.53
E2	0.57	0.56
LogE1	0.28	0.10
LogE2	0.46	0.19
AVE	-19.24	-269.20
R ²	0.62	0.58
Pbias	-1.82	-19.23758
KGE	0.79	0.67417

412

413 Table 2: The objective functions E1, E2, logarithmic versions of E1 and E2, average error
414 (AVG) coefficient of determination R2, Pbias and Kling Gupta efficiency (KGE) (Gupta et al.,
415 2009) used for the surface water calibration (1987-1993) and validation (1994-2007)

416 The J2000 and MODFLOW recharge estimates: With adjustment of hydraulic conductivities
417 from MODFLOW to J2000 it was possible to converge the net recharge estimates between 1.3
418 % with a range of recharge of 0.65-10.03 % for the J2000 and 0.3-11.40 % for MODFLOW.
419 J2000 estimates had an average value of 5.30 % while MODFLOW was 5.20 % for the eight
420 hydraulic zones of the Krom Antonies. The coefficient of determination (R^2) between net
421 recharge from the J2000 and MODFLOW was 0.81. Across the entire dataset J2000
422 overestimated groundwater recharge by 2.75 % relative to MODFLOW, although the
423 coefficient of determination produced an R^2 of 0.92 which is better than during the validation
424 period.



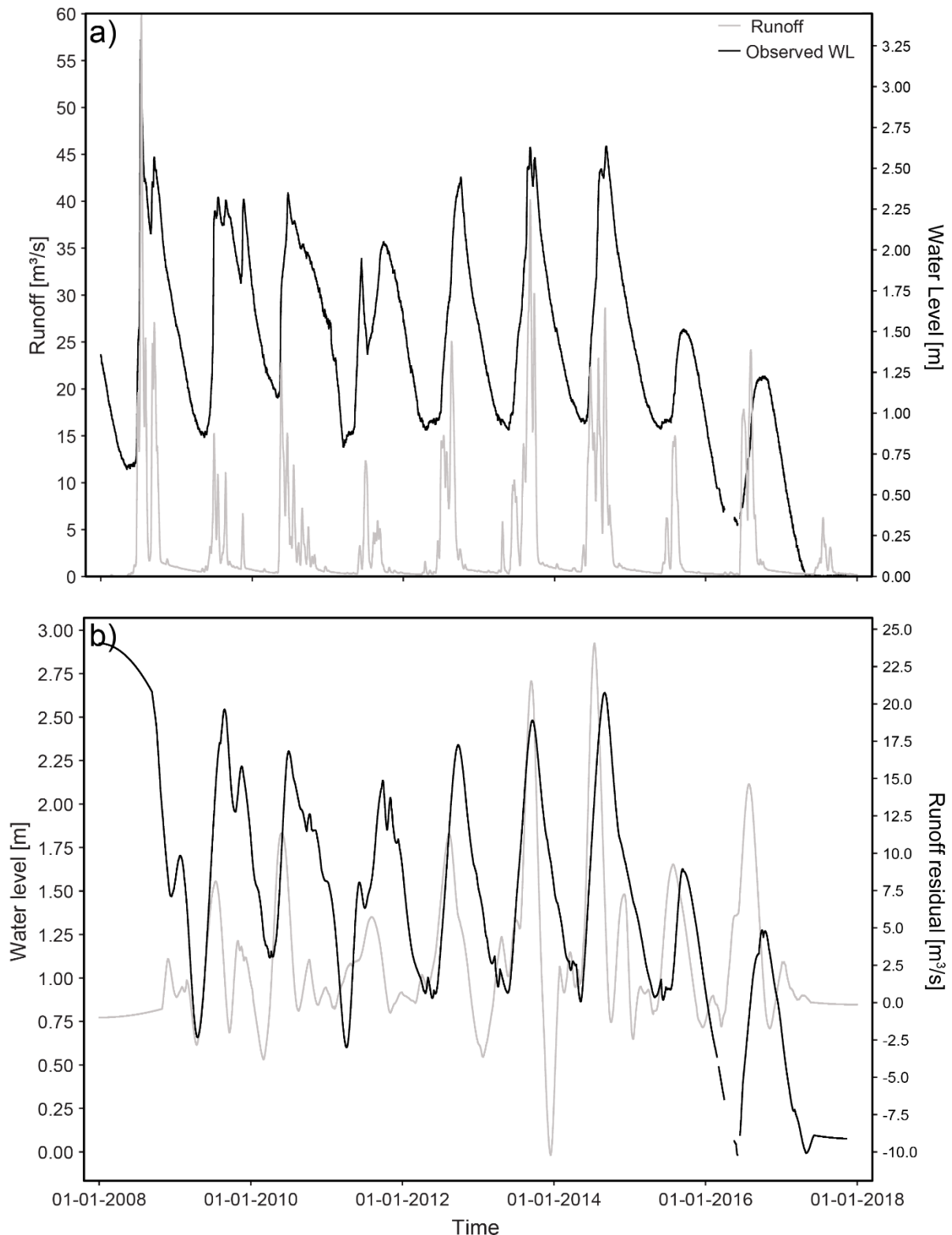
425

426 Figure 7: The groundwater calibration for each hydraulic zone with a) net recharge for the
 427 J2000 and MODFLOW during the model calibration (2016) and b) the net recharge deviation
 428 between MODFLOW and J2000 across the entire modelling timestep (1986-2017)

429 **3.8 EMD filtering**

430 To account for missing streamflow data between 2007-2017, an Empirical Mode
 431 Decomposition (EMD) (Huang et al., 1998) was applied to the measured water level data at
 432 the sub-catchment outlet (G3T001)(Fig. 1) between 1994 to 2018 (Fig 8a). EMD is a method
 433 for the decomposition of nonlinear and nonstationary signals into sub-signals of varying
 434 frequency, so-called intrinsic mode functions (IMF), and a residuum signal. By removing one
 435 or more IMF or the residuum signal, certain frequencies (e.g. noise) or an underlying trend can

436 be removed from the original time series data. This approach was successfully applied to the
437 analysis of river runoff data (Huang et al., 2009) and forecasting of hydrological time series
438 (Kisi et al., 2014). In this study, EMD filtering was used to remove high frequency sub-signals
439 from simulated runoff and measured water level data to compare the more general seasonal
440 variations of both signals (Fig. 8b).



441

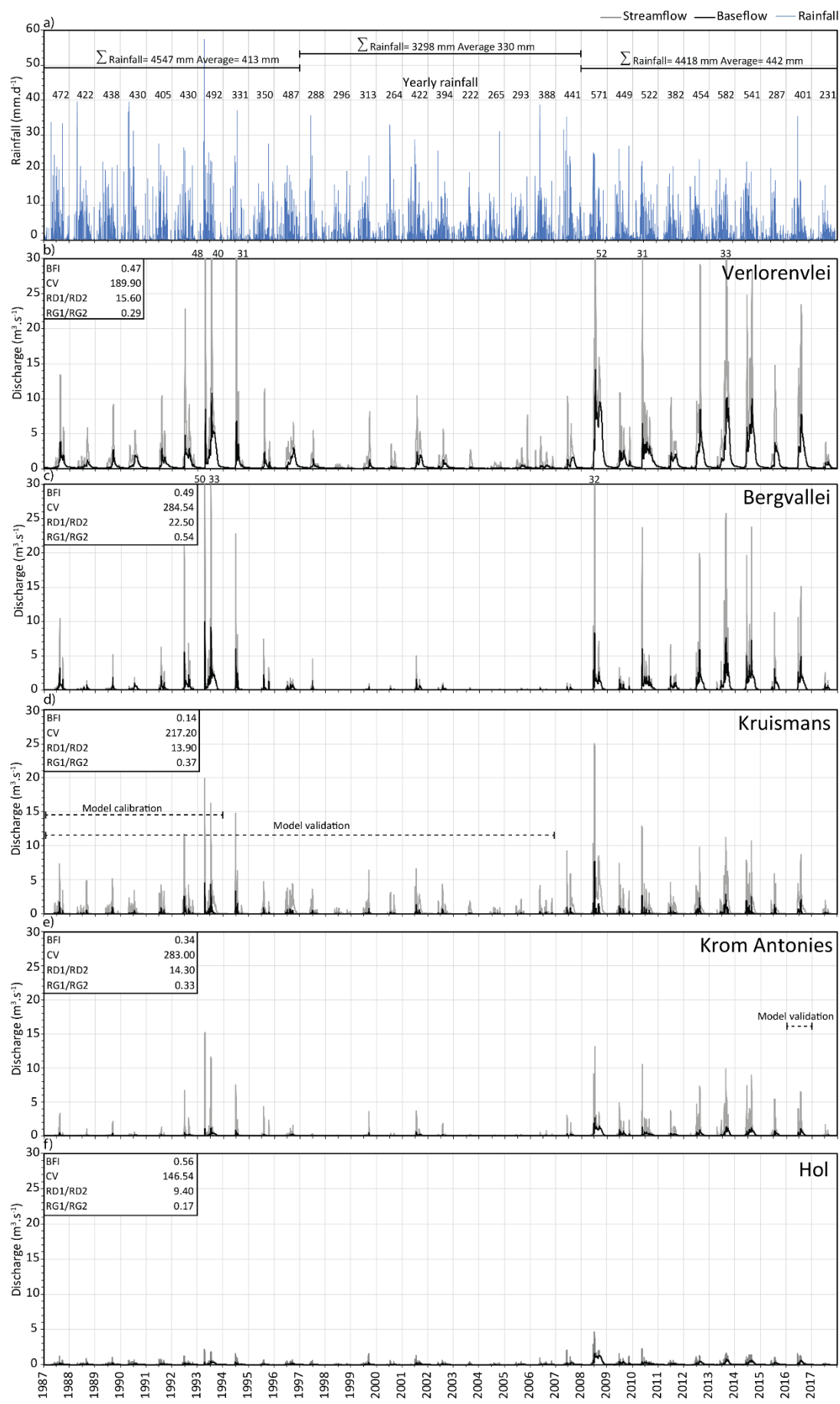
442 Figure 8: a) The water level fluctuations at station G3T001 with modelled runoff and b) the
 443 EMD filtering showing the variation in discharge timeseries attributed a water level change at
 444 the station

445 **4. Results**

446 The J2000 model was used to simulate both runoff and baseflow, with runoff being comprised
447 of direct surface runoff (RD1) and interflow (RD2) and baseflow simulated from the primary
448 (RG1) and secondary aquifer (RG2). Below, the results of the modelled streamflow and
449 baseflow are presented, along with the total flow contribution of each tributary, the runoff to
450 baseflow proportioning and stream exceedance probabilities. The coefficient of variation (CV)
451 was used to determine the streamflow variability of each tributary, while the baseflow index
452 (BFI) was used to determine the baseflow and runoff proportion.

453 **4.1 Streamflow and baseflow**

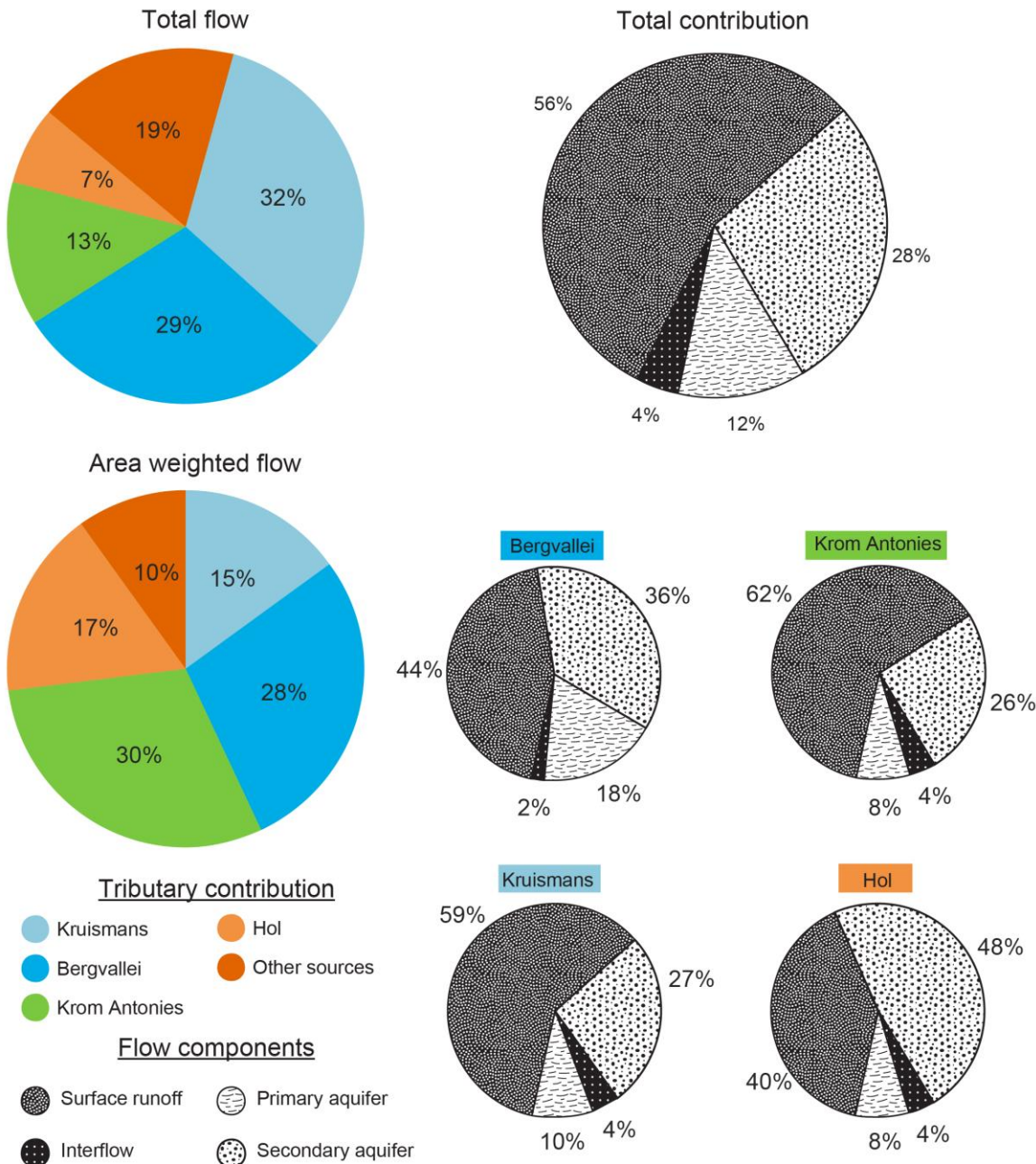
454 Streamflow for the sub-catchment shows two distinctively wet periods (1987-1997 and 2007-
455 2017), separated by a dry period (1997-2007) (Fig. 9). Yearly sub-catchment rainfall volumes
456 between 1987-1997 were between 288 and 492 mm/yr⁻¹, with an average of 404 mm.yr⁻¹. For
457 this period, average yearly streamflow between was 1.4 m³.s⁻¹, with an average baseflow
458 contribution of 0.63 m³.s⁻¹. The modelled streamflow reached a maximum of 48 m³.s⁻¹ in 1993,
459 when 5 m³.s⁻¹ of baseflow was generated after 58 mm of rainfall was received. Between 1997-
460 2007 (dry period) sub-catchment yearly rainfall was between 222 and 394 mm/yr⁻¹ with an
461 average of 330 mm.yr⁻¹ (Fig. 9). For this same period, average yearly streamflow was 0.44
462 m³.s⁻¹, with an average baseflow contribution of 0.18 m³.s⁻¹. The modelled streamflow reached
463 a maximum of 11 m³.s⁻¹ in 2002, with a baseflow contribution of 2.5 m³.s⁻¹ after 28 mm of
464 rainfall was received. During the second wet period between 2007-2017 sub-catchment yearly
465 rainfall was between 231 and 582 mm.yr⁻¹ with an average of 427 mm.yr⁻¹ (Fig. 9). Over this
466 same period, average yearly streamflow was 2.5 m³.s⁻¹ with an average baseflow contribution
467 of 1.3 m³.s⁻¹. The modelled streamflow reached a maximum of 52 m³.s⁻¹ in 2008, with 13 m³.s⁻¹
468 ¹ of baseflow generated after two consecutive rainfall events each of 25 mm.



470 Figure 9: a) Average sub-catchment rainfall between 1987-2017 showing wet cycles (1987-
471 1997 and 2008-2017) and dry cycle (1997-2007), Modelled streamflow and baseflow inflows
472 for the b) Verlorenvlei, c) Bergvallei, d) Kruismans, e) Krom Antonies and f) Hol tributaries
473 with estimated BFI, CV, RD1/RD2, RG1/RG2

474 **4.2 Tributary contributions**

475 The four main feeding tributaries (Bergvallei, Kruismans, Hol and Krom Antonies) together
476 contribute 81% of streamflow for the Verlorenvlei, with the additional 19% from small
477 tributaries near Redelinghuys (Fig. 10). The Kruismans contributes most of the total
478 streamflow at 32 %, but only 15 % of the area-weighted contribution as its sub-catchment is
479 the largest of the four tributaries at 688 km² (Fig. 10). The Bergvallei with a sub-catchment of
480 320 km², contributes 29 % of the total flow with an area weighted contribution of 28 %. The
481 Krom Antonies has the largest area weighted contribution of 30 % due to its small size (140
482 km²) in comparison to the other tributaries, although the Krom Antonies contributes only 13 %
483 of the total flow (Fig. 10). The Hol sub-catchment at 126 km² makes up the smallest
484 contribution to the total flow of only 7 %, but has an weighted contribution of 17 % (Fig. 10).



485

486 Figure 10: The Verlorenvlei reserve flow contributions (total flow and area weighted flow) of
 487 the Kruismans, Bergvallei, Krom Antonies and Hol as well as flow component separation
 488 into surface runoff (RD1), interflow (RD2), primary aquifer flow (RG1) and secondary
 489 aquifer flow (RG2).

490 **4.3 Flow variability**

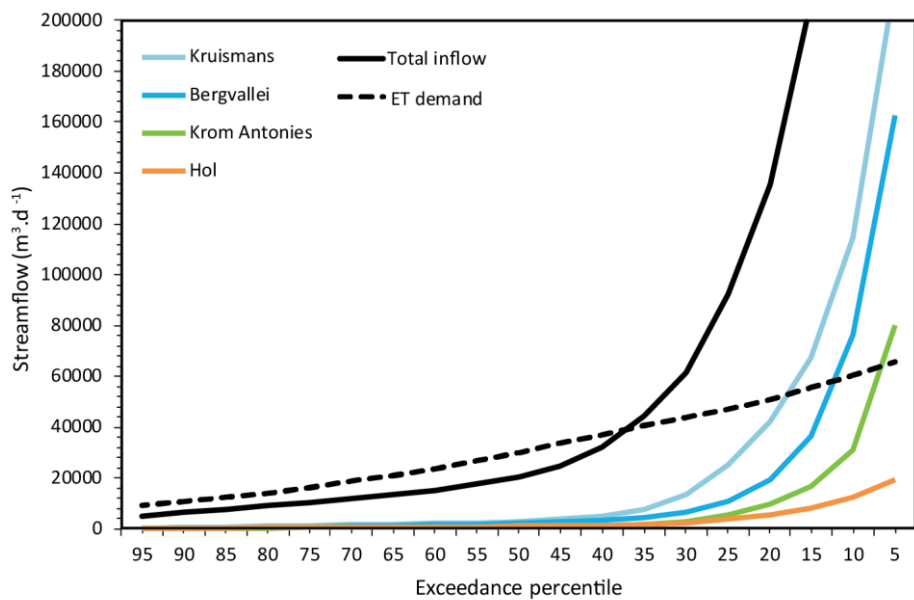
491 Streamflow that enters Verlorenvlei has a large daily variability with a coefficient of variation
492 (CV) of 189.90 (Fig. 9). This is mainly due to high streamflow variability from the Kruismans
493 (32%) with a CV of 217.20, which is the major total flow contributor (Fig 10). The Bergvallei
494 and Krom Antonies, which both have high streamflow variability with CV values of 284.54
495 and 283.00 respectfully (Fig. 9), further contribute to the high variability of streamflow that
496 enters the lake. While the Hol reduces the overall streamflow variability with a CV of 146.54,
497 it is a minor total flow contributor (7%) and therefore does not reduce the overall streamflow
498 variability significantly (Fig. 10).

499 Streamflow that enters Verlorenvlei is dominated by surface runoff which makes up 56 % of
500 total flow, with groundwater and interflow contributing 40 % and 4 % respectfully (Fig. 10).
501 The large surface runoff dominance in streamflow entering the lake, is due to a high surface
502 runoff contribution from the Kruismans and Krom Antonies, which contribute 26 % of total
503 flow from surface runoff. However, for the Bergvallei and Hol, surface runoff contributions
504 are less dominant with 16 % of the total, while the total groundwater contribution is 20 % from
505 these tributaries. Across all four tributaries, the secondary aquifer is the dominant baseflow
506 component with 28 % of total flow, with the primary aquifer contributing 12 %. The Bergvallei
507 and Kruismans contribute the majority of primary aquifer baseflow with 8 % of the total. The
508 secondary aquifer baseflow is mainly contributed by the Kruismans and Bergvallei, where
509 together 18 % of the total is received. Interflow across the four tributaries is uniformly
510 distributed with 0.3 – 1 % of the total flow being contributed from each tributary.

511 **4.4 Flow exceedance probabilities**

512 The flow exceedance probability, which is a measure of how often a given flow is equalled or
513 exceeded was calculated for each of the tributaries as well as the lake water body. The results

514 for the flow exceedance probabilities includes flow volumes which are exceeded 95%, 75%,
 515 50%, 25 % and 5 % of the time. The 95 percentile corresponds to a lake inflow of $0.054 \text{ m}^3 \cdot \text{s}^{-1}$
 516 or $4,702 \text{ m}^3 \cdot \text{d}^{-1}$, with between 0.001 - $0.004 \text{ m}^3 \cdot \text{s}^{-1}$ from the feeding tributaries (Fig. 11 and
 517 Table 3). The 75-percentile flow, which is exceeded 3/4 of the time corresponds to an inflow
 518 of $0.119 \text{ m}^3 \cdot \text{s}^{-1}$ or $10,303 \text{ m}^3 \cdot \text{d}^{-1}$, with between 0.005 - $0.015 \text{ m}^3 \cdot \text{s}^{-1}$ from the feeding tributaries.
 519 Average (50 percentile) streamflow flowing into the Verlorenvlei is $0.237 \text{ m}^3 \cdot \text{s}^{-1}$ or $20,498$
 520 $\text{m}^3 \cdot \text{d}^{-1}$, with between 0.012 - $0.012 \text{ m}^3 \cdot \text{s}^{-1}$ from the feeding tributaries. The 25-percentile flow,
 521 which is exceeded 1/4 of the time corresponds to a lake inflow of $1,067 \text{ m}^3 \cdot \text{s}^{-1}$ or $92,204 \text{ m}^3 \cdot \text{d}^{-1}$
 522 with between 0.044 - $0.291 \text{ m}^3 \cdot \text{s}^{-1}$ from the feeding tributaries. The lake inflows that are
 523 exceeded 5 % of the time correspond to $6.939 \text{ m}^3 \cdot \text{s}^{-1}$ or $599,535 \text{ m}^3 \cdot \text{d}^{-1}$ with between 0.224 -
 524 $2.49 \text{ m}^3 \cdot \text{s}^{-1}$ from the feeding tributaries.



525
 526 Figure 11: The streamflow exceedance percentiles and evaporation demand of the Verlorenvlei
 527 reserve, with the contributions from each feeding tributary

Exceedance percentile	Lake ET	Verlorenvlei		Kruismans		Bergvallei		Krom Antonies		Hol	
	$m^3.d^{-1}$	$m^3.s^{-1}$	$m^3.d^{-1}$	$m^3.s^{-1}$	$m^3.d^{-1}$	$m^3.s^{-1}$	$m^3.d^{-1}$	$m^3.s^{-1}$	$m^3.d^{-1}$	$m^3.s^{-1}$	$m^3.d^{-1}$
95	9158	0.054	4702	0.004	346	0.001	69	0.001	109	0.002	176
90	10956	0.074	6356	0.007	604	0.002	191	0.003	232	0.003	269
85	12559	0.088	7628	0.010	830	0.004	366	0.004	319	0.004	353
80	14249	0.104	8979	0.012	1072	0.007	596	0.005	392	0.005	434
75	16330	0.119	10303	0.015	1291	0.010	839	0.005	459	0.006	508
70	18653	0.136	11759	0.018	1517	0.013	1104	0.006	534	0.007	587
65	21152	0.155	13373	0.021	1791	0.016	1381	0.007	602	0.008	676
60	23791	0.176	15180	0.024	2104	0.019	1657	0.008	685	0.009	786
55	26979	0.203	17575	0.029	2506	0.023	1965	0.009	772	0.011	913
50	30057	0.237	20498	0.035	3032	0.027	2309	0.010	882	0.012	1058
45	33467	0.286	24669	0.043	3755	0.032	2807	0.012	1024	0.014	1222
40	36760	0.371	32023	0.058	5022	0.041	3511	0.015	1258	0.017	1439
35	40391	0.516	44598	0.089	7699	0.053	4613	0.020	1745	0.021	1790
30	43814	0.710	61310	0.156	13511	0.076	6599	0.033	2824	0.029	2481
25	47062	1.067	92204	0.291	25182	0.123	10619	0.062	5387	0.044	3814
20	50997	1.571	135726	0.489	42242	0.223	19295	0.110	9511	0.065	5655
15	55797	2.399	207275	0.780	67408	0.421	36354	0.192	16594	0.096	8262
10	60162	3.759	324746	1.324	114432	0.885	76477	0.359	31045	0.141	12191
5	65418	6.939	599535	2.490	215152	1.884	162795	0.929	80305	0.224	19312

528

529 Table 3: The streamflow exceedance percentiles and lake evaporation demand for the
 530 Verlorenvlei reserve, with the contributions from the Kruismans, Bergvallei, Krom Antonies
 531 and Hol ($m^3.s^{-1}$ and $m^3.d^{-1}$)

532 5. Discussion

533 The adaptation of the J2000 rainfall/runoff model was used to understand the flow
 534 contributions of the main feeding tributaries, the proportioning of baseflow to surface runoff
 535 as well as how often the inflows exceed the lake evaporation demand. Before a comparison
 536 with previous baseflow estimates can be made and the impact of evaporation on the lake
 537 reserves assessed, the model limitations and catchment flow dynamics must also be assessed.

538 5.1 Model limitations and performance

539 A major limitation facing the development and construction of comprehensive modelling
 540 systems in sub-Saharan Africa is the availability of appropriate climate and streamflow data.
 541 For this study, while there was access to over 20 years of streamflow records, the station was

542 only able to measure a maximum of $3.68 \text{ m}^3 \cdot \text{s}^{-1}$, which hindered calibration of the model for
543 high flow events. As such, the confidence in the model's ability to simulate high streamflow
544 events using climate records is limited. While the availability of measured data is a limitation
545 that could affect the modelled streamflow, discontinuous climate records also hindered the
546 estimations of long time series streamflow.

547 Over the course of the 30-year modelling period, a number of climate stations used for
548 regionalisation were decommissioned and were replaced by stations in different areas. This
549 required adaption of climate regionalisation for simulations over the entire 30-year period to
550 incorporate the measured streamflow from the gauging station. To account for missing
551 streamflow records since 2007, an EMD filtering protocol was applied to the runoff data (Fig.
552 6). The results from the EMD filtering showed that after removing the first nine IMFs, the local
553 maxima of both signals match the seasonal water level maxima during most of the years. While
554 considerable improvement can be made to the EMD filtering, the results show some agreement
555 which suggested that the simulated runoff was representative of inflows into the lake.

556 **5.2 Catchment dynamics**

557 Factors that impact on streamflow variability are important for understanding river flow regime
558 dynamics. Previously, factors that affected streamflow variability such as CV and BFI values
559 were used to determine how susceptible particular river systems were to drought (e.g Hughes
560 and Hannart, 2003). While CV values have been used to account for climatic impacts such as
561 dry and wet cycles, BFI values are associated with runoff generation processes that impact the
562 catchment. For most river systems, BFI values are generally below 1 implying that runoff
563 exceeds baseflow. In comparison CV values can be in excess of 10 implying high variability
564 in streamflow volumes (Hughes and Hannart, 2003). In this study, these two measurements

565 have been applied to tributaries as opposed to quaternary river systems, to understand the
566 streamflow input variability into the Verlorenvlei.

567 The highest proportion of streamflow needed to sustain the Verlorenvlei lake water level is
568 received from the Bergvallei tributary, although the area weighted contribution from the Krom
569 Antonies is more significant (Fig. 10). However, CV values for the Bergvallei indicate high
570 streamflow variability. This is partially due to the high surface runoff component in modelled
571 streamflow within the Bergvallei in comparison to the minor interflow contribution, suggesting
572 little sub-surface runoff. While streamflow from the Bergvallei tributary is 54% groundwater,
573 which would suggest a more sustained streamflow, due to the TMG dominance as well as a
574 high primary aquifer contribution, baseflow from the Bergvallei is driven by highly conductive
575 rock and sediment materials. Similarly, CV values for the Krom Antonies indicate high
576 streamflow variability due to the presence of a high baseflow contribution from the conductive
577 TMG and primary aquifers. Although the Krom Antonies has a larger interflow component,
578 which would reduce streamflow variability, the dominant TMG presence within this tributary
579 partially compensates for the subsurface flow contributions.

580 In contrast, the Hol has a much smaller daily streamflow variability in comparison to both the
581 Bergvallei and the Krom Antonies (Fig. 9). While streamflow from the Hol tributary is mainly
582 comprised of baseflow (56%), the dominance of low conductive shale rock formations as well
583 as a large interflow component results in reduced streamflow variability. While the larger shale
584 dominance in this tributary not only results in a more sustained baseflow from the secondary
585 aquifer, it also results in a large interflow component due to the limited conductivity of the
586 shale formations. Compounding the more sustained baseflow from the Hol tributary, the
587 reduced extent of the primary aquifer results in a dominance in slow groundwater flow from
588 this tributary. Similarly, the Kruismans is dominated by shale formations which result in a

589 larger interflow contribution, although due to the limited baseflow contribution (37%) the
590 streamflow from this tributary is highly variable, which impacts on its susceptibility to drought.

591 The results from this study have shown that while the Krom Antonies was initially believed to
592 be the major flow contributor, the Bergvallei is in fact the most significant, although
593 streamflow from the four tributaries is highly variable, with baseflow from the Hol tributary
594 the only constant input source. The presence of conductive TMG sandstones and quaternary
595 sediments in both the Krom Antonies and Bergvallei, results in quick baseflow responses with
596 little flow attenuation. The potential implication of a constant source of groundwater being
597 provided from the Hol tributary, is that if the groundwater is of poor quality this would result
598 in a constant input of saline groundwater, with the Krom Antonies and Bergvallei providing
599 freshwater only after sufficient rainfall has been received.

600 **5.3 Baseflow comparison**

601 The groundwater components of the J2000 model were adjusted using aquifer hydraulic
602 conductivity from a MODFLOW model of one of the main feeding tributaries of the
603 Verlorenvlei. The Krom Antonies was selected as it was previously believed to be the largest
604 input of groundwater to Verlorenvlei (Fig. 2). Baseflow for the Krom Antonies tributary was
605 previously calculated using a MODFLOW model (Watson, 2018), by considering aquifer
606 hydraulic conductivity and average groundwater recharge. As average recharge was used,
607 baseflow estimates from MODFLOW are likely to fall on the upper end of daily baseflow
608 values estimated by the J2000 model. For the Krom Antonies sub-catchment, Watson, (2018)
609 estimated baseflow between 14,000 to 19,000 $\text{m}^3 \cdot \text{d}^{-1}$ for 2010-2016 using MODFLOW. Similar
610 daily baseflow estimates from the J2000 were only exceeded 10 % of the time, with average
611 estimates (50%) of $1,036 \text{ m}^3 \cdot \text{d}^{-1}$ over the course of the modelling period (Fig. 9).

612 The MODFLOW estimates were applied over the course of a wet cycle (2016). In comparison
613 to the MODFLOW estimates (14,000 to 19,000 $\text{m}^3.\text{d}^{-1}$) average baseflow from J2000 for 2016
614 was 8,214 $\text{m}^3.\text{d}^{-1}$. The daily timestep nature of the J2000 is likely to result in far lower baseflow
615 estimates, as recharge is only received over a 6-month period as opposed to a yearly average
616 estimate. One possible implication of this is that while common groundwater abstraction
617 scenarios have been based on yearly recharge, abstraction is likely to exceed sustainable
618 volumes during dry months or dry cycles and this could hinder the ability of the aquifer to
619 supply baseflow. While the groundwater components of the J2000 have been distributed to
620 allow for improved baseflow estimates, the groundwater calibration was applied to the Krom
621 Antonies. However, this study showed that Bergvallei has been identified as the largest water
622 contributor. In hindsight, the use of geochemistry to identify dominant tributaries could have
623 aided the groundwater model adaption. While it would have been beneficial to adapt the
624 groundwater components of the J2000 using the dominant baseflow contributor, considering
625 the geological heterogeneity between tributaries is more important for identifying how to adapt
626 the groundwater components of the J2000. While the distribution of aquifer components
627 improved modelled baseflow, including groundwater abstraction scenarios in baseflow
628 modelling in the sub-catchment is important for future water management for this ecologically
629 significant area.

630 **5.4 The Verlorenvlei reserve and the evaporative demand**

631 For this study, exceedance probabilities were estimated through rainfall/runoff modelling for
632 the previous 30 years within the Verlorenvlei sub-catchment. The exceedance probabilities
633 were determined for each tributary, as well as the total inflows into the lake. These exceedance
634 probabilities were compared with the evaporative demand of the lake, to understand whether
635 inflows are in surplus or whether the evaporation demand exceeds inflow.

636 From the exceedance probabilities generated in this study, the lake is predominately fed by less
637 frequent large discharge events, where on average the daily inflows to the lake do not sustain
638 the lake water level. This is particularly evident in the measured water level data from station
639 G3T001, where measured water levels have a large daily standard deviation (0.62) (Watson *et*
640 *al.*, 2018). With climate change likely to impact the length and severity of dry cycles, it is likely
641 that the lake will dry up more frequently into the future, which could have severe implications
642 on the biodiversity that relies on the lake's habitat for survival. Of importance to the lake's
643 survival is the protection of river inflows during wet cycles, where the lake requires these
644 inflows for regeneration.

645 While the impact of irrigation could not be incorporated, over allocation of water resources
646 may potentially have a significant impact on the catchment water balance, especially during
647 wet cycles when ecosystems are recovering from dry conditions. The increased irrigation
648 during wet cycles as a result of agricultural development, could be a further impact on the
649 recovery of sensitive ecosystems. This type of issue is not limited to Verlorenvlei but applies
650 to many wetlands or estuarine lakes around the world, while they have been classified as
651 protected areas, water resources within the catchments are required for food security. As
652 climate change drives increased temperatures and variability in rainfall, the \pm 10-year cycles
653 of dry and wet conditions may no longer be valid anymore, where these conditions may shorten
654 or lengthen. With the routine breaking of weather records across the world (Bruce, 2018; Davis,
655 2018), it is becoming increasingly evident that conditions are changing and becoming more
656 variable, which could impact sensitive ecosystems around the world, highlighting the need for
657 effective water management protocols during times of limited rainfall.

658

659 **6. Conclusion**

660 Understanding river flow regime dynamics is important for the management of ecosystems that
661 are sensitive to streamflow fluctuations. While climatic factors impact rainfall volume during
662 wet and dry cycles, factors that control catchment runoff and baseflow are key to the
663 implementation of river protection strategies. In this study, groundwater components within
664 the J2000 model were distributed to improve baseflow and runoff proportioning for the
665 Verlorenvlei sub-catchment. The J2000 was distributed using groundwater model values for
666 the dominant baseflow tributary, while calibration was applied to the dominant streamflow
667 tributary. The model calibration was hindered by the DT limit, which reduced the confidence
668 in modelling high flow events, although an EMD filtering protocol was applied to account for
669 the resolution limitations and missing streamflow records. The modelling approach would
670 likely be transferable to other partially gauged semi-arid catchments, provided that
671 groundwater recharge is well constrained. The daily timestep nature of the J2000 model
672 allowed for an in-depth understanding of tributary flow regime dynamics, showing that while
673 streamflow variability is influenced by the runoff to baseflow proportion, the host rock or
674 sediment in which groundwater is held is also a factor that must be considered. The modelling
675 results showed that on average the streamflow influxes were not able to meet the evaporation
676 demand of the lake. High-flow events, although they occur infrequently, are responsible for
677 regeneration of the lake's water level and ecology, which illustrates the importance of wet
678 cycles in maintaining biodiversity levels in semi-arid environments. With climate change likely
679 to impact the length and occurrence of dry cycle conditions, wet cycles become particularly
680 important for ecosystem regeneration, especially for semi-arid regions such as the Verlorenvlei.

681 **7. Acknowledgements**

682 The authors would like to thank the WRC and SASSCAL for project funding as well as the
683 NRF and Iphakade for bursary support. Agricultural Research Council (ARC) and South
684 African Weather Service (SAWS) for their access to climate and rainfall data. The research
685 was carried out in the framework of SASSCAL and was funded by the German Federal
686 Ministry of Education and Research (BMBF) under promotion number 01LG1201E.

687 **8. References**

688 Acreman, M. C. and Dunbar, M. J.: Defining environmental river flow requirements – a review,
689 *Hydrol. Earth Syst. Sci.*, 8(5), 861–876, 2004.

690 Barker, I. and Kirmond, A.: Managing surface water abstraction in Wheater, H. and Kirby,
691 C.(eds) *Hydrology in a changing environment*, vol1, Br. Hydrol. Soc., 249–258, 1998.

692 Batjes, N., Dijkshoorn, K., Van Engelen, V., Fischer, G., Jones, A., Montanarella, L., Petri,
693 M., Prieler, S., Teixeira, E. and Wiberg, D.: Harmonized World Soil Database (version 1.2),
694 Tech. rep., FAO and IIASA, Rome, Italy and Laxenburg, Austria., 2012.

695 Bauer, P., Held, R. J., Zimmermann, S., Linn, F. and Kinzelbach, W.: Coupled flow and salinity
696 transport modelling in semi-arid environments: The Shashe River Valley, Botswana, J.
697 *Hydrol.*, 316(1–4), 163–183, 2006.

698 Bragg, O. M., Black, A. R., Duck, R. W. and Rowan, J. S.: Progress in Physical Geography
699 Approaching the physical-biological interface in rivers : a review of methods, , 4(October
700 2000), 506–531, 2005.

701 Bruce, D.: Prepare for extended severe weather seasons, *Aust. J. Emerg. Manag.*, 33(4), 6,
702 2018.

703 Bunn, S. E. and Arthington, A. H.: Basic principles and ecological consequences of altered
704 flow regimes for aquatic biodiversity, *Environ. Manage.*, 30(4), 492–507, 2002.

705 Conrad, J., Nel, J. and Wentzel, J.: The challenges and implications of assessing groundwater
706 recharge: A case study-northern Sandveld , Western Cape, South Africa, *Water SA*, 30(5), 75–
707 81, 2004.

708 Costanza, R., Arge, R., Groot, R. De, Farberk, S., Grasso, M., Hannon, B., Limburg, K.,
709 Naeem, S., O'Neill, R. V, Paruelo, J., Raskin, R. G., Suttonkk, P. and van den Belt, M.: The
710 value of the world's ecosystem services and natural capital, *Nature*, 387(May), 253–260, 1997.

711 CSIR: Development of the Verlorenvlei estuarine management plan: Situation assessment.
712 Report prepared for the C.A.P.E. Estuaries Programme, , 142, 2009.

713 Davis, G.: The Energy-Water-Climate Nexus and Its Impact on Queensland's Intensive
714 Farming Sector, in *The Impact of Climate Change on Our Life*, pp. 97–126, Springer., 2018.

715 Deb, K., Pratap, A., Agarwal, S. and Meyarivan, T.: A fast and elitist multiobjective genetic
716 algorithm: NSGA-II, *IEEE Trans. Evol. Comput.*, 6(2), 182–197, 2002.

717 Domenico, P. A. and Schwartz, F. W.: *Physical and Chemical Hydrogeology*, John Wiley and
718 Sons, Inc., New York., 1990.

719 DWAF: Sandveld Preliminary (Rapid) Reserve Determinations. Langvlei, Jakkals and
720 Verlorenvlei Rivers. Olifants-Doorn WMA G30. Surface Volume 1: Final Report Reserve
721 Specifications. DWAF Project Number: 2002-227., 2003.

722 Flügel, W.: Delineating hydrological response units by geographical information system
723 analyses for regional hydrological modelling using PRMS/MMS in the drainage basin of the
724 River Bröl, Germany, *Hydrol. Process.*, 9(3-4), 423–436, 1995.

725 Gleick, P. H.: Global freshwater resources: soft-path solutions for the 21st century, *Science*
726 (80-.), 302(5650), 1524–1528, 2003.

727 Harbaugh, Arlen, W.: MODFLOW-2005 , The U . S . Geological Survey Modular Ground-
728 Water Model — the Ground-Water Flow Process, *U.S. Geol. Surv. Tech. Methods*, 253, 2005.

729 Harman, C. and Stewardson, M.: Optimizing dam release rules to meet environmental flow
730 targets, *River Res. Appl.*, 21(2–3), 113–129, 2005.

731 Helme, N.: Botanical report: Fine Scale vegetation mapping in the Sandveld, as part of the
732 C.A.P.E programme., 2007.

733 Huang, N. E., Shen, Z., Long, S. R., Wu, M. C., Shih, H. H., Zheng, Q., Yen, N.-C., Tung, C.
734 C. and Liu, H. H.: The empirical mode decomposition and the Hilbert spectrum for nonlinear
735 and non-stationary time series analysis, in *Proceedings of the Royal Society of London A: mathematical, physical and engineering sciences*, vol. 454, pp. 903–995, The Royal Society.,
736 1998.

737 Huang, Y., Schmitt, F. G., Lu, Z. and Liu, Y.: Analysis of daily river flow fluctuations using
738 empirical mode decomposition and arbitrary order Hilbert spectral analysis, *J. Hydrol.*, 373(1–
739 2), 103–111, 2009.

740 Hughes, D. A.: Providing hydrological information and data analysis tools for the
741 determination of ecological instream flow requirements for South African rivers, *J. Hydrol.*,
742 241(1–2), 140–151, 2001.

743 Hughes, D. A. and Hannart, P.: A desktop model used to provide an initial estimate of the
744 ecological instream flow requirements of rivers in South Africa, *J. Hydrol.*, 270(3–4), 167–
745 181, 2003.

747 Jenson, S. K. and Domingue, J. O.: Extracting topographic structure from digital elevation data
748 for geographic information system analysis, *Photogramm. Eng. Remote Sensing*, 54(11),
749 1593–1600, 1988.

750 Johnson, M. R., Anhaeuesser, C. R. and Thomas, R. J.: *The Geology of South Africa*, Geological
751 Society of South Africa., 2006.

752 Kim, N. W., Chung, I. M., Won, Y. S. and Arnold, J. G.: Development and application of the
753 integrated SWAT-MODFLOW model, *J. Hydrol.*, 356(1–2), 1–16, 2008.

754 King, J. and Louw, D.: Instream flow assessments for regulated rivers in South Africa using
755 the Building Block Methodology, *Aquat. Ecosyst. Health Manag.*, 1(2), 109–124, 1998.

756 Kisi, O., Latifoğlu, L. and Latifoğlu, F.: Investigation of empirical mode decomposition in
757 forecasting of hydrological time series, *Water Resour. Manag.*, 28(12), 4045–4057, 2014.

758 Krause, P.: *Das hydrologische Modellsystem J2000. Beschreibung und Anwendung in großen*
759 *Flussgebieten*, in *Umwelt/Environment*, Vol. 29. Jülich: Research centre., 2001.

760 Krause, P., Boyle, D. P. and Bäse, F.: Comparison of different efficiency criteria for
761 hydrological model assessment, *Adv. Geosci.*, 5, 89–97, 2005.

762 Lynch, S.: Development of a raster database of annual, monthly and daily rainfall for southern
763 Africa, Pietermaritzburg., 2004.

764 Martens, K., Davies, B. R., Baxter, A. J. and Meadows, M. E.: A contribution to the taxonomy
765 and ecology of the Ostracoda (Crustacea) from Verlorenvlei (Western Cape, South Africa),
766 *African Zool.*, 31(1), 22–36, 1996.

767 Meinhardt, M., Fleischer, M., Fink, M., Kralisch, S., Kenabatho, P., de Clercq, W. P., Zimba,
768 H., Phiri, W. and Helmschrot, J.: Semi-arid catchments under change: Adapted hydrological

769 models to simulate the influence of climate change and human activities on rainfall-runoff
770 processes in southern Africa, in Climate change and adaptive land management in southern
771 Africa – assessments, changes, challenges, and solutions, edited by N. Revermann, R.,
772 Krewenka, K.M., Schmiedel, U., Olwoch, J.M., Helmschrot, J. & Jürgens, pp. 114–130, Klaus
773 Hess Publishers, Göttingen & Windhoek., 2018.

774 Muche, G., Kruger, S., Hillman, T., Josenhans, K., Ribeiro, C., Bazibi, M., Seely, M., Nkonde,
775 E., de Clercq, W. P., Strohbach, B., Kenabatho, K. ., Vogt, R., Kaspar, F., Helmschrot, J. and
776 Jürgens, N.: Climate change and adaptive land management in southern Africa – assessments,
777 changes, challenges, and solutions, in Biodiversity & Ecology, edited by R. Revermann, K. M.
778 Krewenka, U. Schmiedel, J. . Olwoch, J. Helmschrot, and N. Jürgens, pp. 34–43, Klaus Hess
779 Publishers, Göttingen & Windhoek., 2018.

780 Nelson, E., Mendoza, G., Regetz, J., Polasky, S., Tallis, H., Cameron, Dr., Chan, K. M. A.,
781 Daily, G. C., Goldstein, J. and Kareiva, P. M.: Modeling multiple ecosystem services,
782 biodiversity conservation, commodity production, and tradeoffs at landscape scales, Front.
783 Ecol. Environ., 7(1), 4–11, 2009.

784 O’Keeffe, J.: Sustaining river ecosystems: Balancing use and protection, Prog. Phys. Geogr.,
785 33(3), 339–357, 2009.

786 Olden, J. D. and Naiman, R. J.: Incorporating thermal regimes into environmental flows
787 assessments: Modifying dam operations to restore freshwater ecosystem integrity, Freshw.
788 Biol., 55(1), 86–107, 2010.

789 Pfannschmidt, K.: Optimierungsmethoden zur HRU-basierten N/A-Modellierung für eine
790 operationelle Hochwasservorhersage auf Basis prognostischer Klimadaten des Deutschen
791 Wetterdienstes: Untersuchungen in einem mesoskaligen Einzugsgebiet im Thüringer Wald,

792 2008.

793 Pfennig, B., Kipka, H., Fink, M., Wolf, M., Krause, P. and Flügel, W.-A.: Development of an
794 extended routing scheme in reference to consideration of multi-dimensional flow relations
795 between hydrological model entities, 18th World IMACS / MODSIM Congr. Cairns, Aust. 13-
796 17 July 2009., 2009.

797 Poff, N. L., Allan, J. D., Bain, M. B., Karr, J. R., Prestegaard, K. L., Richter, B. D., Sparks, R.
798 E. and Stromberg, J. C.: A paradigm for river conservation and restoration, *Bioscience*, 47(11),
799 769–784, 1997.

800 Poff, N. L., Richter, B. D., Arthington, A. H., Bunn, S. E., Naiman, R. J., Kendy, E., Acreman,
801 M., Apse, C., Bledsoe, B. P., Freeman, M. C., Henriksen, J., Jacobson, R. B., Kennen, J. G.,
802 Merritt, D. M., O’Keeffe, J. H., Olden, J. D., Rogers, K., Tharme, R. E. and Warner, A.: The
803 ecological limits of hydrologic alteration (ELOHA): A new framework for developing regional
804 environmental flow standards, *Freshw. Biol.*, 55(1), 147–170, 2010.

805 Postel, S. and Carpenter, S.: Freshwater ecosystem services, *Nature’s Serv. Soc. Depend. Nat.*
806 *Ecosyst.*, 195, 1997.

807 Postel, S. and Richter, B.: Rivers for life: managing water for people and nature, Island Press.,
808 2012.

809 Richter, B. D.: Re-thinking environmental flows: from allocations and reserves to sustainability
810 boundaries, *River Res. Appl.*, 26(8), 1052–1063, 2010.

811 Ridoutt, B. G. and Pfister, S.: A revised approach to water footprinting to make transparent the
812 impacts of consumption and production on global freshwater scarcity, *Glob. Environ. Chang.*,
813 20(1), 113–120, doi:10.1016/j.gloenvcha.2009.08.003, 2010.

814 Rozendaal, A. and Gresse, P. G.: Structural setting of the Riviera W-Mo deposit, western Cape,
815 South Africa, *South African J. Geol.*, 97(2), 184, 1994.

816 Sigidi, N. T.: Geochemical and isotopic tracing of salinity loads into the Ramsar listed
817 Verlorenvlei freshwater estuarine lake , Western Cape , South Africa, (Unpublished MSc
818 thesis) Stellenbosch University., 2018.

819 Sinclair, S., Lane, S. and Grindley, J.: Estuaries of the Cape: Part II: Synopses of available
820 information on individual systems., Stellenbosch., 1986.

821 SRK: Preliminary Assessment of Impact of the Proposed Riviera Tungsten Mine on
822 Groundwater Resources Preliminary Assessment of Impact of the Proposed Riviera Tungsten
823 Mine on Groundwater Resources., 2009.

824 Steudel, T., Bugan, R., Kipka, H., Pfennig, B., Fink, M., de Clercq, W., Flügel, W.-A. and
825 Helmschrot, J.: Implementing contour bank farming practices into the J2000 model to improve
826 hydrological and erosion modelling in semi-arid Western Cape Province of South Africa,
827 *Hydrol. Res.*, 46(2), 192, 2015.

828 UMVOTO-SRK: Reconnaissance investigation into the development and utilization of the
829 Table Mountain Group Artesian Groundwater, using the E10 catchment as a pilot study area.,
830 2000.

831 Wagener, T. and Wheater, H. S.: Parameter estimation and regionalization for continuous
832 rainfall-runoff models including uncertainty, *J. Hydrol.*, 320(1–2), 132–154, 2006.

833 Watson, A. P.: Using distributive surface water and groundwater modelling techniques to
834 quantify groundwater recharge and baseflow for the Verlorenvlei estuarine system , west coast
835 , South Africa, (Unpublished PhD thesis) Stellenbosch University., 2018.

836 Watson, A. P., Miller, J. A., Fleischer, M. and de Clercq, W. P.: Estimation of groundwater
837 recharge via percolation outputs from a rainfall/runoff model for the Verlorenvlei estuarine
838 system, west coast, South Africa., *J. Hydrol.*, 558(C), 238–254, doi:10.1016/S1532-
839 0464(03)00032-7, 2018.

840 Willems, P.: A time series tool to support the multi-criteria performance evaluation of rainfall-
841 runoff models, *Environ. Model. Softw.*, 24(3), 311–321, doi:10.1016/j.envsoft.2008.09.005,
842 2009.

843 Wishart, M. J.: The terrestrial invertebrate fauna of a temporary stream in southern Africa,
844 *African Zool.*, 35(2), 193–200, 2000.

845